I&EC research
Industrial & Engineering Chemistry Research
pubs.acs.org/IECR
Article

Key Properties and Parameters of Pd/CeO_2 Passive NO_x Adsorbers

Alessandra Toso, Maila Danielis, Carla de Leitenburg, Marta Boaro, Alessandro Trovarelli, and Sara Colussi*

Cite This: *Ind. Eng. Chem. Res.* 2022, 61, 3329−3341
Read Online

ABSTRACT: In this paper, a series of Pd/CeO_2 catalysts prepared by different synthesis routes and showing different morphological and textural properties have been investigated for passive NO_x adsorption (PNA) applications. The results obtained by NO_x adsorption/desorption tests demonstrated that NO_x storage capacity and NO_x storage efficiency of Pd/CeO_2 materials depend strictly on their surface area, whereas the morphology of the support and the Pd deposition method do not seem to play a key role. In contrast, the Pd deposition method does impact the dynamics of NO_x desorption by affecting the amount of NO_x desorbed at different temperatures. This seems to be connected to Pd−Ce interactions at the nanoscale that favor NO_x desorption at higher temperatures suitable for PNA application. These findings are relevant in designing and optimizing the properties of Pd/CeO_2 materials for their function as passive NO_x adsorbers.

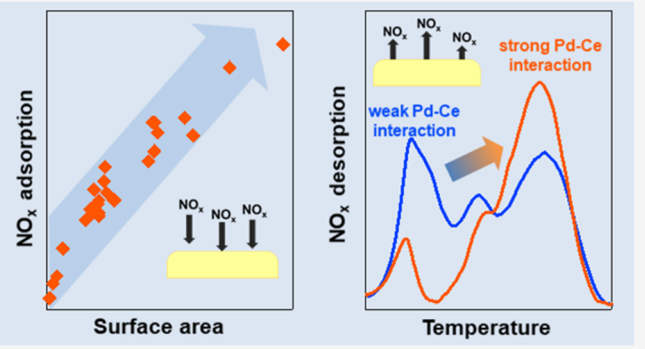

1. INTRODUCTION

The regulation of NO_x (NO and NO_2) emissions from gasoline and diesel engines is becoming more stringent due to the growing concern about their effects on the environment and human health.[1,2] Selective catalytic reduction (SCR) and lean NO_x traps (LNTs) are the current technologies developed and commercialized for the NO_x emission abatement on diesel vehicles. In SCR systems, NO_x are reduced to N_2 using ammonia derived from urea decomposition and using catalyst formulations based on vanadia−titania or on metal-substituted zeolites.[3−5] LNTs consist of precious metals (typically Pt), alkali, or alkaline earth metals (K or Ba) dispersed on high surface area (HSA) support (Al_2O_3 or CeO_2−Al_2O_3) and work under switching lean/rich conditions. During lean operation, NO_x are stored as nitrites/nitrates and then converted to N_2 and released during the rich cycle.[6,7] However, especially for diesel engines, the cold start period emissions represent a concerning issue. In diesel engines, in fact, the warm-up rate is slow and a relatively long time is required (ca. 2−3 min) for the SCR system to reach its optimal operating temperature (ca. 473 K), resulting in a large amount of NO_x emitted at tailpipe. Moreover, urea injection and decomposition requires a temperature typically higher than 423 K, making the SCR system unsuitable for NO_x reduction at low temperature.[8] Also, for the LNT system, the trapping efficiency is poor (below 473 K), and the regeneration of LNTs requires fuel injection, resulting in lower fuel efficiency.[7]

An approach to overcome the low-temperature issues of both SCR technology and lean NO_x traps is the use of passive NO_x adsorbers (PNAs): a PNA should adsorb the NO_x emitted from the engine during a cold start period and release them when NO_x are efficiently converted in the SCR device, i.e., above 473 K.[9,10] In 2001, Ford Motor Company first reported the combination of a Pt-Al_2O_3 passive NO_x adsorber with SCR to efficiently reduce NO_x emissions.[11] More recently, Honda and Johnson Matthey developed novel materials, referred to as N-TWC material and Cold Start Concept (CSC), respectively, for low-temperature HCs and/or NO_x trapping based on Pd/zeolites.[12,13] In the literature, zeolites-based adsorbers and metal oxide-supported materials have been studied for low-temperature NO_x storage.[9,10,14−20] Palladium is usually the metal of choice for PNAs, as it is capable of promoting NO_x storage in the form of more labile nitrites that can desorb at lower temperatures, whereas Pt tends to oxidize NO giving rise to adsorbed nitrate species that are not released in the working range of PNAs.[16,21] Pd/zeolites (BEA, MFI, SSZ-13) are promising candidates for PNA applications, and in general are considered more robust with respect to oxide-based adsorbers, especially for their resistance to sulfur poisoning.[10,20] However, they still present some unresolved issues, such as dealumination following high-temperature hydrothermal treatments[22] and deactivation in presence of CO, which causes the agglomeration of Pd^{2+} into

Received: December 8, 2021
Revised: February 12, 2022
Accepted: February 14, 2022
Published: February 23, 2022

https://doi.org/10.1021/acs.iecr.1c04805
Ind. Eng. Chem. Res. 2022, 61, 3329−3341

large PdO clusters.[20] On the other hand, oxide-based materials containing redox-active components, primarily CeO_2, are usually regarded as very interesting due to their well-known NO_x storage ability even at room temperature,[23,24] hydrothermal resistance, and different storage mechanisms compared to zeolites.[25] The poor sulfur tolerance is the main drawback of these materials but the unique oxygen storage capacity and redox behavior of ceria make it hardly replaceable in many applications,[26,27] and recently various solutions have been proposed in the literature to increase its resistance to sulfur poisoning.[28−30] Moreover, different authors observed an improvement of NO_x adsorption capacity in the presence of CO on ceria-containing materials,[18,31,32] as well as an increase of NO_x desorption temperature in a suitable window for SCR when ceria was added to a Pd/zeolite formulation.[33] Another interesting aspect of Pd/CeO_2 adsorbers is that, different from zeolites, they are sensitive to the NO/NO_2 ratio, the presence of NO_2 promoting NO adsorption.[25] This condition is particularly relevant for fast SCR applications, where an optimal NO/NO_2 ratio (1:1) is required for the SCR system.[5,34]

In the case of zeolites, much effort has been devoted to the correlation of NO_x adsorption/desorption properties with the nature of Pd active sites and support framework, especially regarding the spatial arrangement and electronic properties of Pd species, and the pore size and volume.[15,19,21,35] However, to the best of our knowledge, the correlation between morphological and textural properties of Pd/CeO_2 materials and passive NO_x storage has not yet been fully elucidated. In this paper, different synthesis approaches have been employed to prepare 1 wt % Pd/CeO_2 materials with different morphological features. Their adsorption capacity and desorption dynamics have been studied in correlation with their texture and morphology. The overall results shed some light on the understanding of the link between material properties and NO_x adsorption/desorption behavior of Pd/CeO_2 materials.

2. EXPERIMENTAL SECTION

2.1. Catalyst Preparation. A series of 1 wt % Pd/CeO_2 samples have been prepared following different synthesis approaches and using different ceria supports. We have used two commercial ceria samples, denoted as CeO_2 A and CeO_2 B, and three polycrystalline ceria powders prepared in our laboratory (CeO_2 LA, CeO_2 HSA1, and CeO_2 HSA2). CeO_2 LA was synthesized by ammonia precipitation in the presence of lauric acid; CeO_2 high surface area 1 (HSA1) and CeO_2 high surface area 2 (HSA2) were both prepared following a hydrothermal route to favor the formation of a high surface area material.[36] Ceria powders with controlled morphology, CeO_2 nanocubes (CeO_2 NC), and nanorods (CeO_2 NR) were also prepared by hydrothermal synthesis. All ceria supports were calcined at 823 K for 3 h prior to Pd deposition, unless otherwise specified (details of the synthesis procedure for all samples are reported in the Supporting Information). Palladium (1% by weight) was loaded by conventional incipient wetness impregnation using a $Pd(NO_3)_2$ solution (Sigma-Aldrich) or by dry mechanical milling of Pd black and ceria powders following a procedure developed in our laboratory.[37] The materials prepared by impregnation were dried and calcined at 823 K for 3 h before use, whereas samples prepared by milling were not treated further. We prepared also a Pd/CeO_2 sample by solution combustion synthesis (SCS) using urea as a reducing agent (all of the details for the preparation of Pd-loaded materials are reported in the Supporting Information). On selected samples, a hydrothermal aging (HA) treatment was performed by exposing the material to wet (10 vol % H_2O) flowing air at 1073 K for 16 h. Another aging treatment was performed on a few catalysts at 1173 and 1473 K for 3 h under static air. The materials were named using the sample code reported in Scheme 1: frame 1 indicates the method used to incorporate

Scheme 1. Sample Code Used for Pd/CeO_2 Materials

1	2	3
Pd(iw)	Ce(HSA1)823	F

Pd on CeO_2 (iw: incipient wetness, m: milling, SCS: solution combustion synthesis); frame 2 indicates the support code and the calcination temperature before the introduction of Pd, frame 3 states if the material has been used as prepared in the fresh state (F), after hydrothermal aging (HA) or after aging treatment at 1173 K (A1173) or at 1473 K (A1473). Table S1 summarizes the preparation route and sample code for all of the materials considered in this work.

2.2. Catalyst Characterization. The Brunauer−Emmett−Teller (BET) surface area and porosity measurements were carried out by nitrogen adsorption/desorption at 77 K in a Micromeritics Tristar 3000 apparatus. Each sample (~250 mg) was previously outgassed under vacuum at 423 K for 2 h to remove adsorbed contaminants. The powder was then cooled under vacuum to 77 K before dosing N_2 on the sample at incremental steps. The evaluation of the adsorption/desorption branches of the isotherm and the hysteresis between them provides information about the size and volume of pores; BET and Barrett−Joyner−Halenda (BJH) methods were employed for the calculation of surface area and pore size distribution, respectively.

X-ray powder diffraction (XRD) analysis was performed on a Philips X'Pert diffractometer equipped with an X'Celerator detector, using Ni-filtered Cu Kα radiation (λ = 1.542 Å) and operating at 40 kV and 40 mA, with a step size of 0.02° and 40 counts per step.

High-resolution transmission electron microscopy (HRTEM) images were collected on a JEOL 2010 F instrument equipped with a field emission gun at an accelerator voltage of 200 kV.

Temperature programmed reduction (TPR) experiments have been performed to study the redox properties of Pd/ceria materials. TPR measurements were carried out in a Micromeritics Autochem II apparatus by loading 50 mg of sample in a U-shaped quartz reactor supported over a quartz wool bed. Before the reduction, the catalyst was pretreated in air at 623 K for 1 h. Then, the samples were cooled to 193 K using liquid nitrogen and a gaseous N_2 purge for 10 min. Afterward, the gas was switched to a mixture of 5% H_2/N_2 (35 mL/min), and the temperature was increased up to 1173 K at a ramp rate of 10 K/min while monitoring hydrogen consumption with a thermal conductivity detector (TCD).

In situ diffuse reflectance infrared Fourier transformation spectroscopy (DRIFTS) measurements have been carried out to analyze the reaction intermediates during the NO_x adsorption/desorption cycle. DRIFT spectra have been recorded on a Fourier transform infrared (FT-IR) spectrometer (Thermo Scientific Nicolet iS-50 FTIR) equipped with a

https://doi.org/10.1021/acs.iecr.1c04805
Ind. Eng. Chem. Res. 2022, 61, 3329−3341

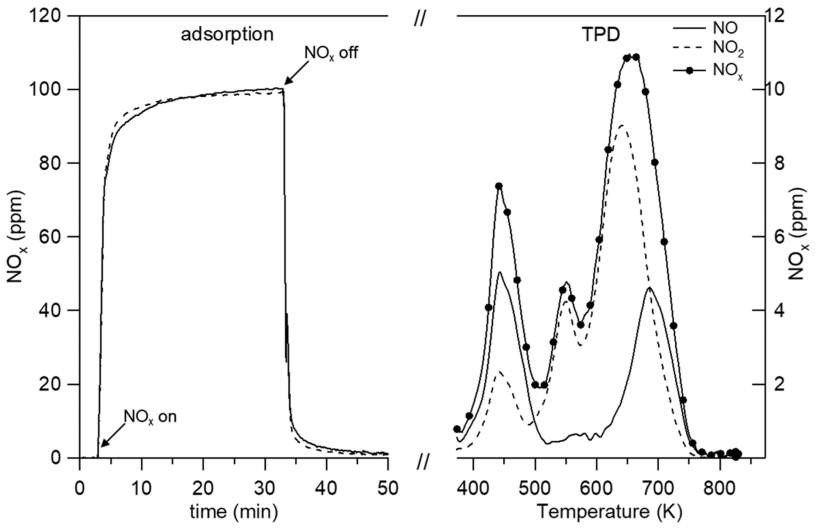

Figure 1. NO and NO_2 profiles during the NO_x adsorption/desorption cycle.

deuterated triglycine sulfate (DTGS) detector. The catalyst powder was loaded into a Pike cell closed with a KBr window. Reaction gases were mixed by mass flow controllers before introduction into the IR cell. The temperature of the reaction cell was controlled by a K-type thermocouple. The spectrometer was continuously purged with dry nitrogen to avoid the diffusion of air into the system. Prior to NO_x adsorption, each sample was pretreated in lean conditions (8% O_2 in N_2) at 723 K for 10 min. Then, the sample was cooled to 373 K, collecting a background spectrum every 50 K from 723 to 373 K in the same reaction atmosphere (100 scans with a resolution of 4 cm^{-1}). NO (100 ppm) and 100 ppm NO_2 were introduced at 373 K for 30 min at a flow rate of 100 mL/min, recording the DRIFT spectra every 2 min (32 scans with a resolution of 4 cm^{-1}); then, NO and NO_2 were switched off, leaving the samples in N_2 for 45 min. Similar experiments were carried out by feeding only 100 ppm NO or NO_2 in N_2 (or 8% O_2). To evaluate the thermal stability of the stored NO_x species, temperature programmed desorption (TPD) was performed in N_2 (or 8% O_2) from 373 up to 723 K with a ramp rate of 10 K/min. Spectra collected during TPD were referred to the background spectrum recorded at the same temperature after the pretreatment. Nicolet OMNIC software was employed to analyze the DRIFT spectra.

2.3. NO_x Adsorption/Desorption Tests. NO_x adsorption/desorption tests were carried out in a laboratory setup capable of treating the samples under a lean/rich atmosphere (see scheme in Figure S1). Each sample (30 mg) was loaded in the powder form in a quartz microreactor on a quartz wool bed. The inlet and outlet gas compositions were analyzed with an online MKS 2030 MultiGas FT-IR Analyzer. Before NO_x adsorption, two different pretreatments were used to understand the effect of the oxidation state of the catalyst on NO_x adsorption/desorption performance. During lean preconditioning, the sample was exposed to an oxidizing atmosphere (8% O_2, 10% CO_2, 5% H_2O balance N_2) at 823 K for 10 min, while the rich pretreatment consisted in the exposure to a CO-containing atmosphere (2000 ppm CO, 10% CO_2, 5% H_2O, balance N_2) at 723 K for 20 min. For NO_x adsorption studies, an equimolar NO/NO_2 ratio was employed to understand the effect of the simultaneous presence of NO and NO_2 since it has been reported that on ceria-based materials, (i) NO_2 adsorbs more easily than NO[31] and (ii) the presence of NO_2 favors NO adsorption, differently from zeolites.[25] Moreover, an equimolar NO/NO_2 ratio corresponds to the optimal conditions for the fast SCR reaction.[5,34] NO_x storage measurements were performed at 373 K by feeding 100 ppm NO, 100 ppm NO_2, 8% O_2, 10% CO_2, and 5% H_2O in N_2 for 30 min. Then, NO_x was switched off until no more NO_x were detected at the outlet (about 40−45 min). To evaluate NO_x desorption behavior, temperature-programmed desorption (TPD) was carried out from 373 to 823 K with a heating rate of 10 K/min in a lean atmosphere (8% O_2, 10% CO_2, 5% H_2O, balance N_2). For pretreatments and NO_x adsorption/desorption tests, the total flow rate was maintained at 400 mL/min. The experimental protocol used to investigate NO_x storage/release performance is reported in Figure S2.

Figure 1 shows the profile of NO and NO_2 concentrations during the adsorption/desorption for a typical experiment. The NO_x storage capacity was calculated as the difference between the area/integral of NO_x breakthrough curves measured bypassing the reactor and that of NO_x breakthrough curves measured during adsorption, as reported in the following equation

$$NO_x^{stored} = \int_0^t [NO_x^{in}]\,dt - \int_0^t [NO_x^{out}]\,dt$$

where $\int_0^t [NO_x^{in}]\,dt$ and $\int_0^t [NO_x^{out}]\,dt$ represent the total amount of NO_x fed to the system and NO_x measured at the outlet of the reactor, respectively, during the 30 min adsorption step at 373 K. Partial NO_x storage was also calculated after 1 min of NO_x exposure since usually the cold-start period is of ca. 2−3 min. The adsorption capacity was calculated as the amount of NO_x (NO + NO_2) adsorbed in milligrams per gram of sample (mg NO_x/g).

NO_x storage efficiency (hereafter referred to as NSE) was calculated as the ratio between NO_x stored and NO_x fed to the reactor, as reported below

$$NSE = \frac{NO_x^{stored}}{\int_0^t [NO_x^{in}]\,dt} \times 100$$

https://doi.org/10.1021/acs.iecr.1c04805
Ind. Eng. Chem. Res. 2022, 61, 3329−3341

Table 1. Textural Properties of the Samples Considered in This Study

sample #	sample name	BET surface area (m^2/g)	pore volume (cm^3/g)	average pore size (Å)	isotherm type
1	Pd(m)Ce(HSA2)623F	249	0.272	38	II
2	Pd(iw)Ce(HSA2)623F	193	0.251	41	II
3	Pd(m)Ce(HSA1)823F	159	0.204	40	II
4	Pd(iw)Ce(HSA1)823F	146	0.186	39	II
5	Pd(iw)Ce(A)823F	117	0.294	71	I
6	Pd(iw)Ce(HSA1)923F	114	0.205	53	II
7	Pd(m)Ce(A)823F	113	0.272	71	I
8	Pd(iw)Ce(B)823F	112	0.437	126	III
9	Pd(m)Ce(B)823F	107	0.414	127	III
10	Pd(iw)Ce(NR)823F	72	0.29	137	III
11	Pd(iw)Ce(A)823HA	64	0.26	122	I
12	Pd(SCS)CeF	62	0.06	43	IV
13	Pd(iw)Ce(B)823HA	61	0.36	191	III
14	Pd(m)Ce(B)823HA	55	0.32	196	III
15	Pd(m)Ce(LA)823F	55	0.26	168	III
16	Pd(m)Ce(B)1173F	55	0.30	178	III
17	Pd(iw)Ce(LA)823F	54	0.16	98	III
18	Pd(iw)Ce(HSA2)623HA	50	0.203	123	I
19	Pd(m)Ce(HSA2)623HA	49	0.230	146	I
20	Pd(iw)Ce(HSA1)823HA	47	0.16	105	II
21	Pd(m)Ce(B)823A1173	46	0.30	213	III
22	Pd(m)Ce(A)823HA	41	0.202	167	I
23	Pd(iw)Ce(NC)823F	17	0.14	269	IV
24	Pd(iw)Ce(NR)823HA	11	0.05	197	III
25	Pd(m)Ce(B)1473F	7	0.02	109	III
26	Pd(m)Ce(B)823A1473	3	0.01	69	III

The amount of NO and NO_2 released during TPD was calculated from the integral of the corresponding TPD curve as a function of time.

3. RESULTS AND DISCUSSION

3.1. Material Characterization. Table 1 shows the textural characteristics of all materials investigated in this study. For each sample, the type of hysteresis loop during nitrogen adsorption/desorption cycles, according to IUPAC classification, is reported as an index of the pore geometry in the mesoporous materials.[38] Figure S3 shows the hysteresis loop for some representative materials.

The surface area of the investigated materials ranges from ca. 250 m^2/g to values as low as <10 m^2/g in samples aged at high temperatures. As expected, fresh samples prepared from CeO_2 HSA2 show the highest BET surface areas, with Pd(m)Ce(HSA2)623F having the highest value due to the low calcination temperature of the support before the introduction of Pd (623 K). The fresh samples supported on commercial ceria powders prepared by incipient wetness (Pd(iw)Ce(A)823F and Pd(iw)Ce(B)823F) and dry milling (Pd(m)Ce(A)823F and Pd(m)Ce(B)823F) as well as those prepared on polycrystalline CeO_2 (Pd(iw)Ce(HSA1)823F and Pd(m)Ce(HSA1)823F) show intermediate surface area values, followed by fresh Pd(iw)Ce(NR)823F, Pd(SCS)CeF, and Pd(iw)Ce(LA)823F. The lowest surface area for fresh samples is that of Pd(iw)Ce(NC)823F, as expected when ceria is prepared in the form of nanocubes.[39] Inside these main groups based on the surface area, the difference arises from the size and shape of the pores, which depend on the type of CeO_2 used and are only slightly influenced by the Pd deposition method. A consistent drop in the surface area and pore volume is observed for samples calcined at high temperatures (Pd(m)Ce(B)1173F and Pd(m)Ce(B)1473F). Pd(SCS)CeF shows also a very small pore volume likely due to high temperatures reached locally during the solution combustion synthesis.[40] The distribution of pores for some selected Pd/CeO_2 samples is reported in the Supporting Information (Figure S4). Overall, the pore size distribution is quite narrow, with the exception of fresh samples supported on Ce(B)823, but also in this case a well-defined maximum is visible.

Most of the fresh Pd/CeO_2 samples display a type III hysteresis, which corresponds to slit-shape pores on platelike particles.[38] Pd-based materials supported on ceria with high surface area (Pd(iw)Ce(HSA1)823F and Pd(iw)Ce(HSA1)-923F) show, instead, an adsorption/desorption isotherm of type II, typical of materials with disordered pore distribution and shape. On fresh samples, the hysteresis of type I, specific of cylindrical-like pores, is observed only for Pd(iw)Ce(A)823F. Type IV hysteresis, associated to narrow pore channels, is exhibited by Pd(SCS)CeF and Pd(iw)Ce(NC)823F. Hydrothermal aging causes a consistent drop of the surface area and pore volume for all the considered materials, but the type of porosity is generally maintained with respect to the corresponding fresh catalysts.

The crystal structure of Pd/CeO_2 samples was investigated by XRD analysis (Figures S5 and S6). The shape and the intensity of the diffraction peaks of CeO_2 depend on the calcination temperature of the support or on the temperature of the aging treatment. The trend of CeO_2 crystal sizes calculated by Scherrer's equation (Table S2, Supporting Information) is in good agreement with that of the surface area, i.e., samples with a higher surface area show smaller crystallites compared to those with lower surface area. A small diffraction peak at 40.2° relative to metallic Pd is present on a few samples prepared by milling, whereas on the fresh

https://doi.org/10.1021/acs.iecr.1c04805
Ind. Eng. Chem. Res. 2022, 61, 3329−3341

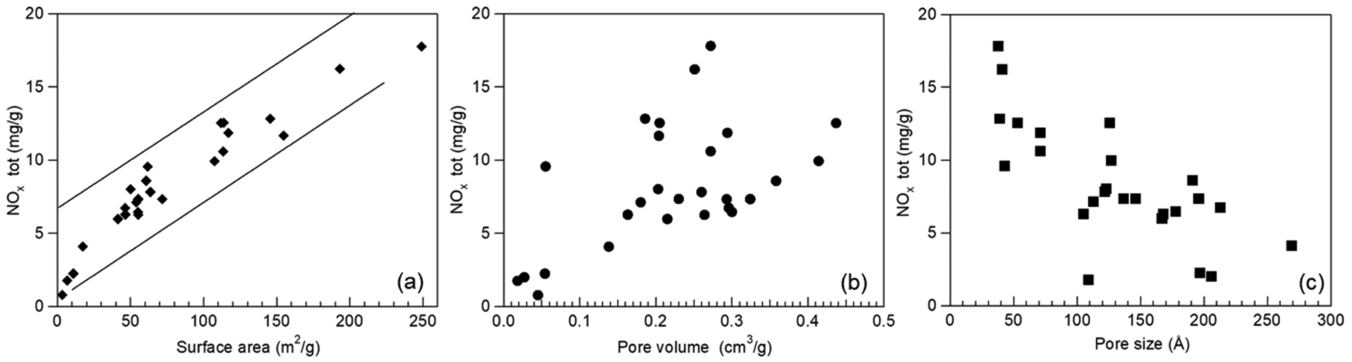

Figure 2. Dependence of the overall NO_x storage capacity (after 30 min) on the (a) surface area, (b) pore volume, and (c) pore size for all samples considered in this work.

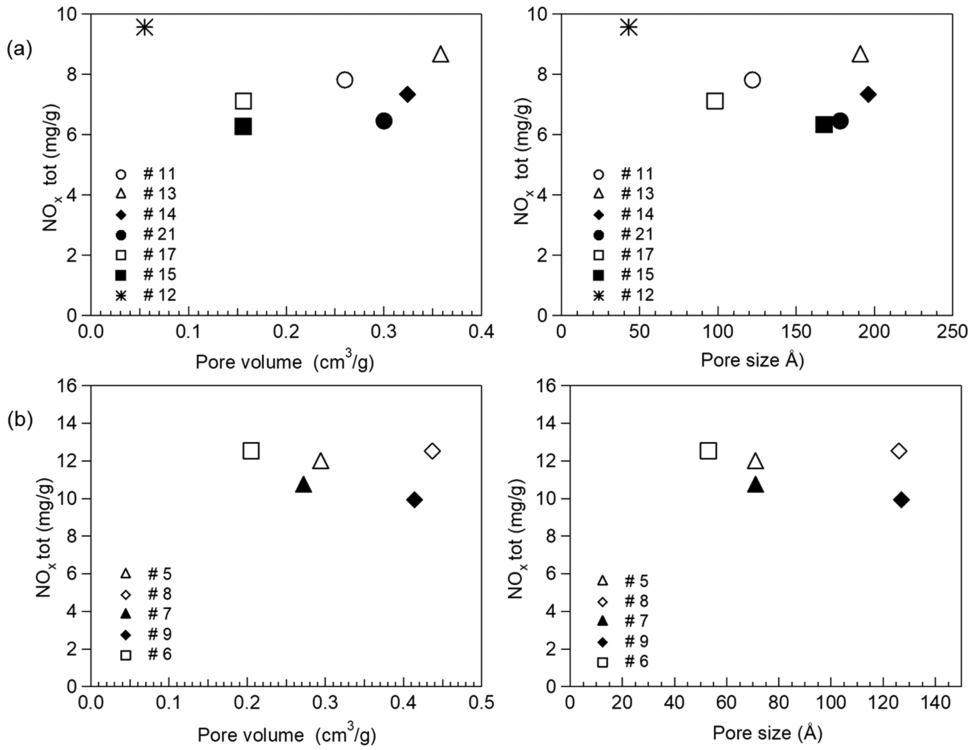

Figure 3. NO_x adsorption capacity at 30 min after lean pretreatment versus the pore volume (left) and pore size (right) on samples with surface areas in the range of (a) 54−64 m^2/g and (b) 97−117 m^2/g (the sample number is listed in Table 1).

impregnated samples no peaks belonging to Pd or PdO are detected. On the basis of previous HRTEM characterization of the low-surface area Pd/CeO_2 catalysts prepared in our lab, on milled samples, the Pd features observed might be due to a few Pd agglomerates not spread uniformly on the support during the milling process. On the high-surface-area Pd/CeO_2 samples prepared by dry milling, neither Pd nor PdO nanoparticles were observed (Figure S7). This might be due to the presence of palladium embedded into the outermost layers of ceria crystallites and/or in highly dispersed form, as previously reported.[37]

3.2. NO_x Adsorption. Herein, only the results obtained from NO_x adsorption/desorption tests after lean pretreatment are shown, unless otherwise stated. The quantitative analysis is reported in the Supporting Information (see Tables S3 and S4).

The samples tested in this work show very different adsorption capacities, ranging from 0.78 to 17.8 mg/g (Table S3). Such a variety allows finding correlations between the textural/morphological properties of the materials and their adsorption behavior. In Figure 2, the overall NO_x storage measured on fresh and aged samples is plotted against the BET surface area, pore volume, and pore size.

Looking at Figure 2a, the correlation between the surface area and the amount of stored NO_x is almost linear, as the increase of the surface area corresponds to an increase of NO_x storage capacity, and this is observed irrespective of the material preparation, the aging treatment, and the palladium deposition method (Table S3). After aging, NO_x adsorption capacity decreases significantly (Table S3), consistently with the decrease of the surface area.

Regarding the pore size and volume of the samples, the correlation with the amount of stored NO_x is not so evident as in the case of the surface area (Figure 2b,c). For example, Figure 2b shows that materials having similar pore volumes (in the range of 0.25 cm^3/g) have very different adsorption

https://doi.org/10.1021/acs.iecr.1c04805
Ind. Eng. Chem. Res. 2022, 61, 3329−3341

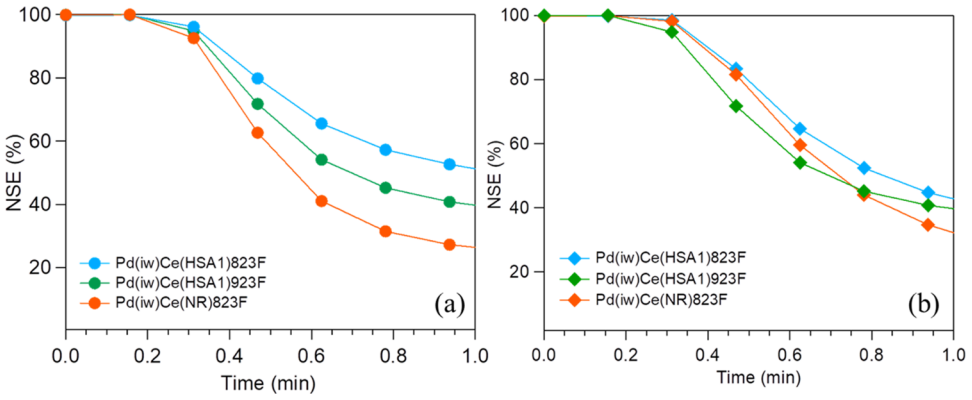

Figure 4. NO_x storage efficiency over time as a function of surface area after (a) lean pretreatment and (b) rich pretreatment for some selected Pd/CeO_2 samples.

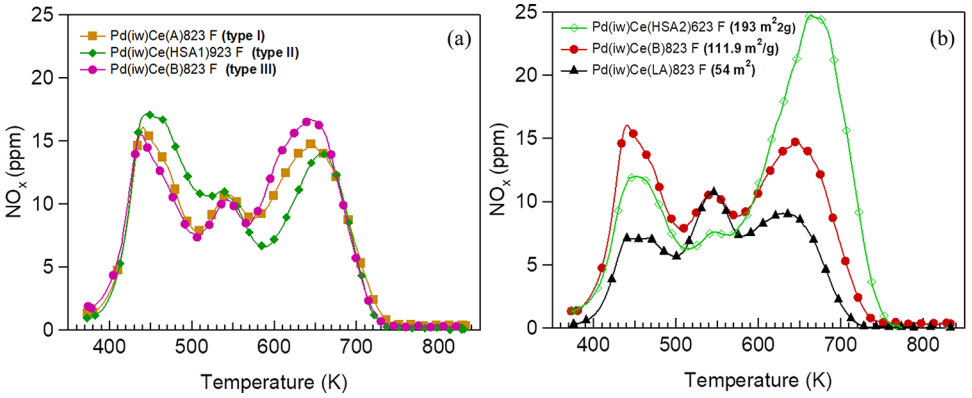

Figure 5. NO_x release profile on Pd/CeO_2 samples with (a) similar surface areas and different porosities (types I−III according to the IUPAC classification) and (b) different surface areas.

capacities, ranging from 6 to 16 mg/g, excluding a relevant effect of this parameter in NO_x adsorption. The same result can be inferred for the effect of pore size, where a NO_x adsorption capacity of 2−12 mg/g is observed for an average pore size value in the range 110−130 Å. The above findings are more evident considering materials with similar surface areas, thus ruling out the effect of this parameter on their adsorption capacity. Figure 3 shows the NO_x adsorption against pore size and volume in samples with similar surface area; results confirm that the overall NO_x storage is not significantly affected by pore size and volume.

When Pd/CeO_2 samples are pretreated under reducing conditions, the relationship between the amount of NO_x stored and the surface area is still linear, although the linearity is lost for samples with the highest surface area values (Figure S8a). With respect to the pore volume and size, again, the correlation between NO_x adsorption capacity and geometry of pores is not straightforward. The results obtained for the series of Pd/CeO_2 adsorbers allow one to infer that the structural properties, in particular the pore size, are not so relevant as in the case of zeolite-based PNAs. For Pd supported on zeolites, in fact, pore size was found to play a key role in determining NO_x storage capacity; in particular, Pd/zeolites having large pores were able to store a higher amount of NO_x.[15,22,35] One important property that has to be considered in NO_x adsorption over CeO_2 is the presence of oxygen vacancies that can act as preferential adsorption sites for both NO and NO_2.[16,24] The reducibility of the oxide support is in fact regarded as a key factor for the activity and stability of PNAs, and the presence of oxygen vacancies has been related to a decrease in the formation of stable nitrates.[9,21] Figure 4a,b shows the NO_x storage efficiency against adsorption time for three representative samples with different surface area values (surface areas ranging from 72 to 146 m^2/g) and different redox behavior (quantified from TPR analysis reported in Figure S9 and Table S5). After lean pretreatment, the NSE is proportional to the surface area and independent of the adsorption time, while, after rich pretreatment, NSE is initially higher for Pd(iw)Ce(NR)823F and reaches a value close to that observed under lean conditions after 1 min. This can be explained by considering that, initially, the presence of oxygen vacancies, promoted by rich pretreatment, can positively affect the storage of NO_x. However, the oxidative atmosphere during adsorption restores a situation similar to that observed after lean pretreatment, and the NSE of Pd(iw)Ce(NR)823F decreases faster than that observed on the other reference samples, suggesting that as time progresses the surface area, and thus the rate of active sites saturation, prevails over the redox capacity of CeO_2 in determining NO_x storage efficiency. Therefore, although the different degrees of CeO_2 reduction after rich pretreatment can affect NO_x uptake, this is evident only at the initial stage of adsorption affecting only slightly the total NO_x adsorption at longer times.

Summarizing the data obtained by screening various Pd/CeO_2 materials, NO_x storage capacity and the NO_x storage efficiency against time depend mainly on the surface area of samples, although after rich pretreatment the reducibility of the support might play a role at least in the initial stages of

https://doi.org/10.1021/acs.iecr.1c04805
Ind. Eng. Chem. Res. 2022, 61, 3329−3341

adsorption, whereas the size, volume, and shape of pores play a negligible role on the overall amount of adsorbed NO_x.

3.3. NO_x Desorption. From a practical point of view, passive NO_x adsorbers should be able to release the stored NO_x under oxidizing conditions as the temperature increases during driving operation, and ideally above 473 K where the SCR catalyst becomes effective. The dynamics of NO_x desorption was studied by temperature-programmed desorption (TPD) from 373 to 823 K. After lean pretreatment, the overall amount of NO_x desorbed is almost equal to the amount of NO_x stored during the adsorption (Table S3). On the contrary, after rich pretreatment (Table S4) of all samples, the amount of desorbed NO_x is lower than that of stored NO_x, likely due to the further reduction of nitrogen oxides to N_2 catalyzed by reduced Ce^{3+} sites.[24,41] However, an attempt to carry out the experiment using He as a carrier gas and following the desorption with a mass spectrometer did not provide useful results in this respect. Figure 5a,b shows the evolution of NO_x during desorption at increasing temperatures on some representative Pd/CeO_2 samples.

Figure 5a shows the TPD profile of impregnated materials having different porosities but similar surface areas. The desorption of NO_x takes place in three different steps, with maxima at around 450, 550, and 650 K. For all of the three samples, NO_x starts to desorb at 373 K with a large peak in the range 373−473 K. With increasing temperatures, other two desorption peaks are present: a smaller one between 503 and 573 K, and a larger one between 573 and 773 K. The dynamics of NO_x release does not seem to be affected by different characteristics of the material, and a slight difference among the samples arises only from the amount of NO_x desorbed in each step, especially above 573 K. This suggests that species with similar adsorption strengths were formed during the adsorption step at 373 K, irrespective of the type of porosity. The surface area does not affect the dynamics of NO_x desorption but only the amount of NO_x released in agreement with the higher NO_x adsorbed. This is illustrated in Figure 5b, where the desorption of samples with different surface areas is reported. The observed NO_x−TPD curves differ from profiles reported in the literature for CeO_2-based materials, where only one or two desorption peaks are usually identified.[16,42,43] The difference might be attributed to the use of a full NO_x (NO + NO_2) mixture in the present case, instead of using only NO. Indeed, an experiment carried out by feeding 170 ppm NO and 30 ppm NO_2 (see the Figure S10, Supporting Information) shows only two desorption peaks during TPD. Moreover, it has to be mentioned that in the literature the addition of up to 24% NO_2 did not result in any additional desorption feature but only in the increase of the two peaks.[25]

Figure 6 shows the effect of the palladium deposition method on the NO_x desorption curves; the comparison is carried out between conventional impregnated (Pd(iw)Ce(A)823F, Pd(iw)Ce(B)823F), milled (Pd(m)Ce(A)823F, Pd(m)Ce(B)823F), and solution combustion synthesized (Pd(SCS)CeF) samples. The temperature of 523 K was fixed as a parameter to evaluate the desorption efficiency of Pd/CeO_2 materials, as for passive NO_x adsorption applications the desirable desorption temperature should be located in the operating window of the SCR system (above 473 K).

Again, irrespective of the preparation route, three distinct NO_x release peaks are detected; however, for impregnated Pd/CeO_2 samples the fraction of NO_x released below 523 K is much higher with respect to their corresponding samples

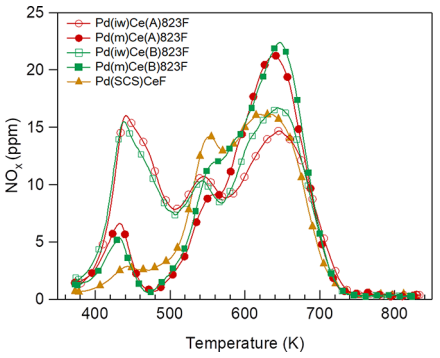

Figure 6. NO_x desorption profiles for some selected impregnated, milled, and SCS Pd/CeO_2 samples after lean pretreatment.

prepared by dry milling on the same ceria support. Also, on Pd(SCS)CeF, a larger amount of adsorbed NO_x is released above 523 K compared to the samples prepared by incipient wetness impregnation. Figure 7a,b shows the amount of NO_x desorbed at low and high temperatures (with respect to the reference temperature of 523 K) on impregnated and milled samples, respectively.

It is evident that all samples prepared by dry milling and the one prepared by the solution combustion synthesis desorb a larger amount of NO_x at higher temperatures compared to conventional impregnated materials, irrespective of the textural characteristics of ceria. This feature is observed also after rich pretreatment (Figures S11 and S12). The change in NO_x desorption dynamics is tentatively attributed to Pd−Ce interactions that favor the formation of more stable adsorbed species in samples where Pd is deposited by dry milling or by solution combustion synthesis. In our group, we have reported that preparing a Pd-ceria catalyst by solution combustion synthesis can give rise to an ordered Pd−O−Ce superstructure over the ceria surface[40] and, more recently, that the low-energy milling of Pd and polycrystalline CeO_2 powders leads to a strong redox exchange between Pd and CeO_2, resulting in highly reactive and stable Pd−O−Ce sites.[37,44] In both configurations, the presence of these highly reactive sites might promote the formation of nitrates, more thermally stable than nitrites, resulting in a lower amount of NO_x desorbing below 523 K on milled and SCS samples with respect to the impregnated ones. This conclusion is supported by the separate NO and NO_2 desorption profiles reported in Figure 8. It is clear that, on Pd(iw)Ce(A)823F, the stored NO_x are mainly released as NO in the range of 373−523 K, whereas, in the same temperature range on the milled sample, NO desorption is much lower and NO_2 is predominant above 523 K.

Both milled and impregnated samples are able to desorb almost all of the stored NO_x in isotherm conditions at 593 K (see Figure S13 and Table S6, Supporting Information), with only a minimum amount of NO_x that requires a temperature of about 700 K to be completely removed. The main difference among samples remains linked to the amount of NO_x desorbing between 473 and 593 K, i.e., the optimal window for the SCR system (see Table S6). Additional experiments carried out by feeding NO or NO_2 only (Figure S14 and Tables S7 and S8) indicate the higher tendency of the impregnated sample in desorbing NO_x in the form of NO, especially at lower temperatures, and the lower NO adsorption capacity of the milled sample.

https://doi.org/10.1021/acs.iecr.1c04805
Ind. Eng. Chem. Res. 2022, 61, 3329−3341

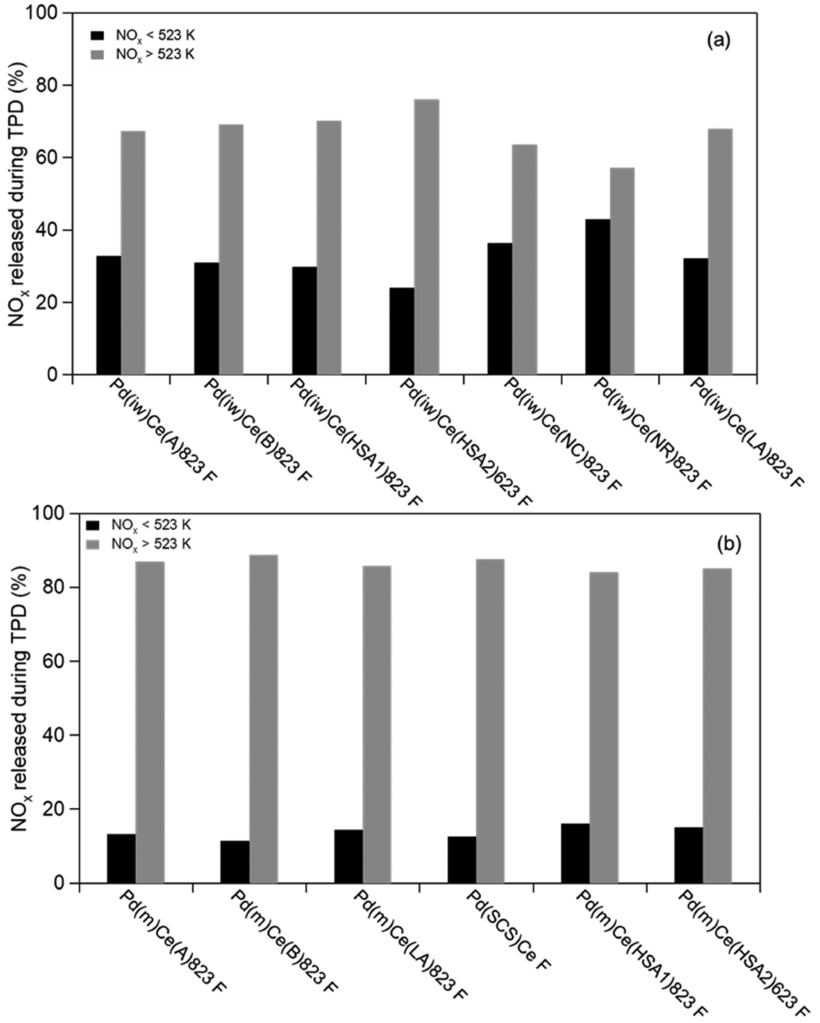

Figure 7. Amount of NO_x desorbed below and above 523 K for selected samples with different Pd−ceria interactions: (a) impregnated samples and (b) milled and SCS samples.

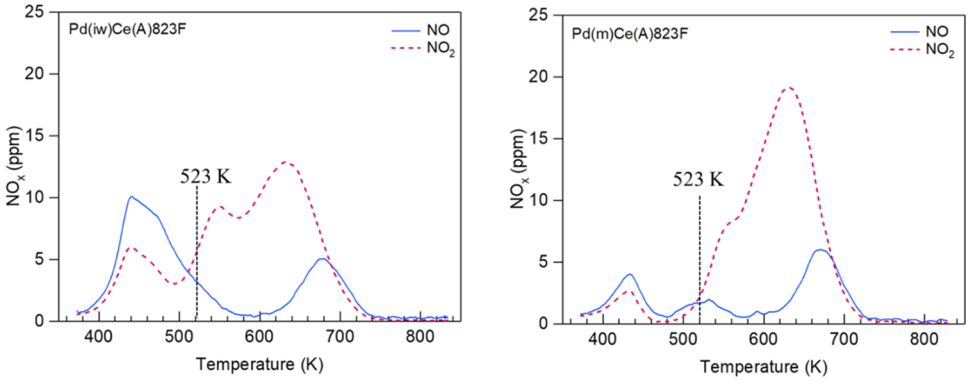

Figure 8. NO and NO_2 release profiles during TPD on Pd(iw)Ce(A)823F and Pd(m)Ce(A)823F after lean pretreatment.

3.4. FT-IR Studies. To further elucidate the different dynamics of NO_x desorption on milled and impregnated samples and, thus, the different NO_x desorption efficiency, DRIFT measurements have been performed on Pd(iw)Ce(A)823F and Pd(m)Ce(A)823F, selected as reference materials. Adsorption and desorption experiments have been carried out by feeding NO or NO_2 separately in an oxidizing atmosphere (8 vol % O_2) after lean pretreatment. DRIFT patterns are reported in absorbance mode, as it can be considered almost proportional to the concentration of adsorbed species on the surface. It should be noted that these experiments do not reproduce exactly the operating conditions of the reactor setup because it was not possible to feed water in the DRIFT cell, due to its KBr window, and the co-presence of CO_2 (and H_2O) would have made it difficult to interpret the DRIFT patterns due to the overlapping of nitrite/nitrate and carbonate/hydroxyl bands. However, the results obtained using these simplified conditions are still representa-

https://doi.org/10.1021/acs.iecr.1c04805
Ind. Eng. Chem. Res. 2022, 61, 3329−3341

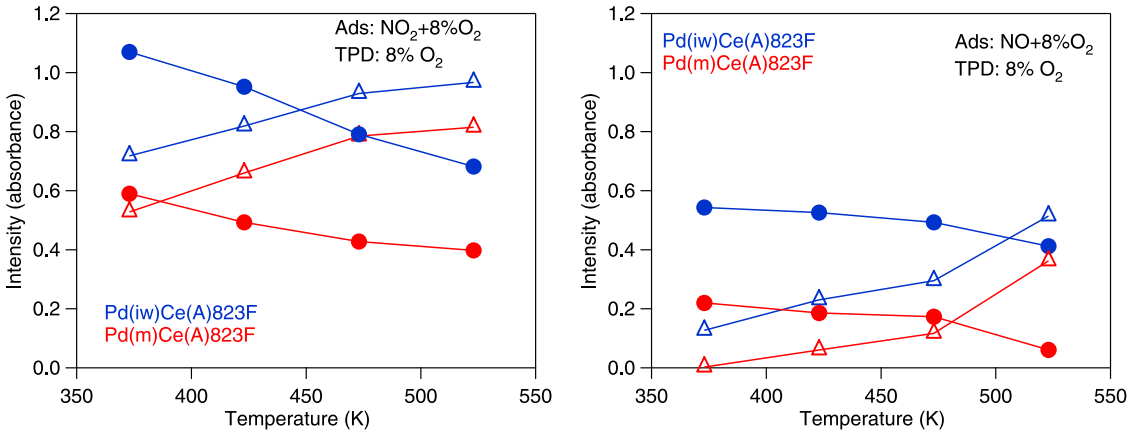

Figure 9. Evolution of (●) nitrites (1350−1050 cm^{-1}) and (△) nitrates (1500−1590 cm^{-1}) as a function of temperature during TPD (8 vol % O_2) on Pd(iw)Ce(A)823F and Pd(m)Ce(A)823F after NO_2 (left) and NO (right) adsorption.

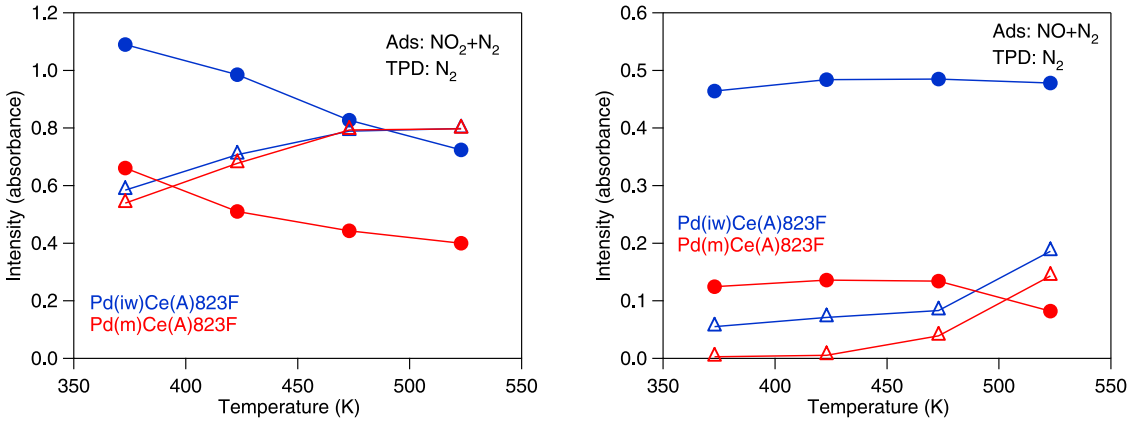

Figure 10. Evolution of (●) nitrites (1350−1050 cm^{-1}) and (△) nitrates (1500−1590 cm^{-1}) as a function of temperature during TPD (N_2) on Pd(iw)Ce(A)823F and Pd(m)Ce(A)823F after NO_2 (left) and NO (right) adsorption.

tive of the behavior observed in the reactor, especially regarding the dynamics of NO_x desorption (Table S9). From the literature, it is clear that the reaction atmosphere has an impact on NO_x adsorption/desorption, particularly on the amount of NO_x stored and released that is inhibited by the presence of H_2O and CO_2,[43,45] but less on the desorption dynamics,[43] which is the focus of our DRIFT experiments. In the presence of only NO (Figure S15a), after 30 min of adsorption on the milled sample, only the bands belonging to bidentate nitrites on ceria are observed (~1170 cm^{-1} with a corresponding band at 1310 cm^{-1}), whereas for the impregnated sample also weaker bands of bidentate or bridged nitrates (1529, 1552 cm^{-1}) are detected.[46−48] When only NO_2 is fed (NO_2 + 8 vol % O_2), the IR patterns are different and more complex on both samples, including more evident features in the nitrate region between 1590 and 1500 cm^{-1} (Figure S15b). In the case of Pd(iw)Ce(A)823F, at 373 K, NO_x are mainly stored as bidentate nitrites (1176, 1310 cm^{-1}) and bridged nitrites (1217 cm^{-1}) on CeO_2. Additional weaker bands are observed at 830, 1100, 1359, and 1370 cm^{-1}, which could be attributed to nitrites or hyponitrites species.[41,46,49] Also, monodentate (1458, 1033 cm^{-1}), bidentate, or bridged nitrates (1604, 1529, 1552, 1013 cm^{-1}) are present.[47,48] Starting from this situation, the mutual evolution of IR bands was followed during TPD in the presence of 8 vol % O_2 (Figure S16), and the relative semiquantitative analysis is depicted in Figure 9 for the nitrite (1350−1050 cm^{-1}) and nitrate regions (1590−1500 cm^{-1}). Overall, the results collected during desorption show that on Pd(m)Ce(A)823F the surface is mostly populated by nitrates at lower temperatures compared to Pd(iw)Ce(A)823F when only NO_2 is adsorbed. After NO adsorption, the situation is different but again on the milled sample, the population of nitrites and nitrates becomes closer at 473 K, whereas for the impregnated sample at this temperature the surface is still mostly covered by nitrites. Moreover, for Pd(m)Ce(A)823F, the reciprocal trend of NO_2^- and NO_3^- clearly indicates that the latter is formed at the expense of surface nitrites for both NO and NO_2 adsorptions. For the impregnated sample, the interconversion takes place after NO_2 adsorption, whereas after NO exposure the surface coverage of nitrites and nitrates is roughly constant up to 473 K.

Trying to discriminate the effect of oxygen availability for each sample, similar experiments have been carried out by feeding NO or NO_2 only in an inert atmosphere (N_2 flow) after pretreating the samples in a lean atmosphere (8 vol % O_2), and monitoring NO_x desorption in N_2. TPD spectra are reported in Figure S17 for impregnated and milled samples, respectively, and semiquantitative analysis is shown in Figure 10. The absence of oxygen has a more relevant impact on Pd(iw)Ce(A)823F with respect to Pd(m)Ce(A)823F, as shown by the comparison of the mutual evolution of nitrite and nitrate bands in Figures 9 and 10.

https://doi.org/10.1021/acs.iecr.1c04805
Ind. Eng. Chem. Res. 2022, 61, 3329−3341

To better highlight the contribution of each oxidant (O_2 and/or NO_2), the crossover temperature (T at which the exchange between the intensity of NO_2^- and NO_3^- IR bands takes place) is plotted as a function of feed oxidizing potential in Figure 11 for each sample. On Pd(m)Ce(A)823F, the

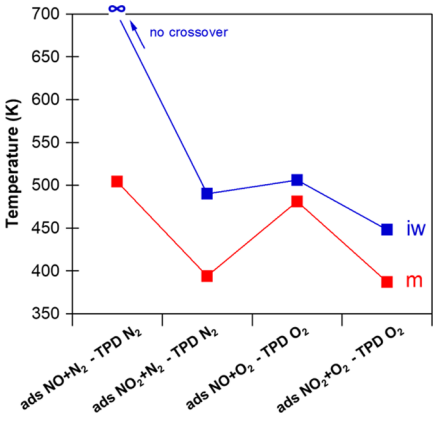

Figure 11. Crossover temperatures after NO and NO_2-only adsorption in inert and oxidizing atmospheres for Pd(iw)Ce(A)823F and Pd(m)Ce(A)823F.

crossover temperature is always lower than on Pd(iw)Ce(A)-823F, highlighting the higher tendency of the milled sample to convert nitrites to nitrates. Comparing the temperatures under inert gas, it appears that the milled sample is almost not affected by the absence of oxygen, likely thanks to the presence of labile lattice oxygen, which is available to a higher extent on the disordered surface structure of milled Pd/CeO_2 materials.[37]

Preliminary results for simultaneous NO + NO_2 adsorption (100 ppm NO, 100 ppm NO_2, in N_2) at 373 K are reported in Figure S18, showing a series of DRIFT spectra collected during TPD in an inert atmosphere. The IR bands are similar to those observed in the presence of NO_2 only (described above) and indicate a general interconversion of nitrite and nitrate species. However, by looking at the semiquantitative analysis reported in Figure 12, it can be observed that on the impregnated sample, at 373 K, NO_x are mainly stored as nitrites; above 423 K, nitrites start to decrease and, at the same time, the intensity of nitrates grows. At 523 K, nitrites and nitrates show the same absorbance, suggesting that they are present in an equal amount on the catalytic surface. Also on the milled sample, nitrate bands start to increase as the temperature increases, but this happens at the expense of nitrites, becoming the predominant surface species at 473 K, as clearly illustrated in Figure 12. Moreover, at 523 K, NO_x are mainly present as nitrates rather than nitrites. This dynamics resembles that observed in Figure 10 when feeding NO_2 only in nitrogen, indicating that NO_2 has a major effect on the overall NO_x adsorption/desorption process.

Tentative experiments carried out by adsorbing NO_x in the reactor with the full mixture (100 ppm NO, 100 ppm NO_2, 8% O_2, 10% CO_2, 5% H_2O in N_2) and following desorption by DRIFTS did not provide straightforward results due to the overlapping of carbonate/hydroxyl bands with those of nitrites/nitrates. However, the milled sample presented a lower surface coverage and a higher nitrates/nitrites ratio at 373 K, in contrast with that observed on the impregnated one. This closely resembles that observed under NO_2 and NO only

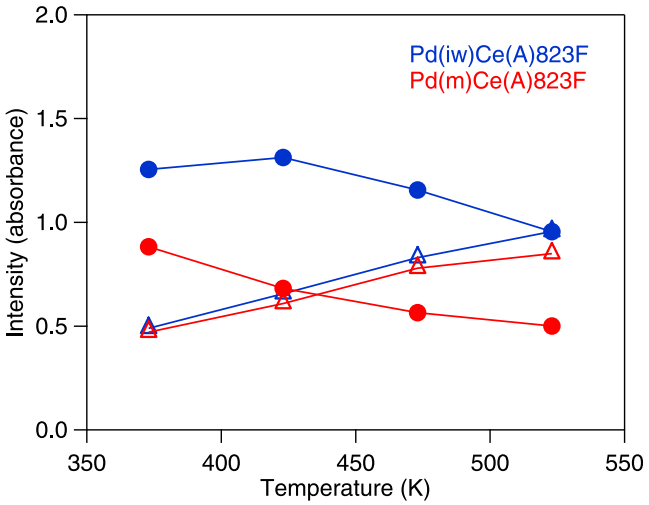

Figure 12. Evolution of (●) nitrites (1350−1050 cm^{-1}) and (△) nitrates (1500−1590 cm^{-1}) as a function of temperature during TPD in N_2 on Pd(iw)Ce(A)823F and Pd(m)Ce(A)823F after NO + NO_2 adsorption in N_2.

experiments (Figures 9, 10, and 12), allowing a correlation between DRIFT measurements and NO_x desorption followed in the reactor setup.

Overall, these findings corroborate the possibility that Pd−O−Ce sites on the highly defective surfaces and related mobile oxygen, formed upon strong Pd/ceria interaction during mechanical milling as already reported in our previous works,[37,44] are more effective in oxidizing nitrites to nitrates. By coupling the results of DRIFT measurements described above and TPD profiles (Figure 8), NO_x release peaks below 523 K can be attributed to the desorption of nitrites and hyponitrites species, as also reported by other authors.[41,43] These species are less thermally stable than nitrates and are present in larger amounts on Pd(iw)Ce(A)823F.

The dynamics of formation/decomposition of nitrites and nitrates and their interconversion during desorption appear to be controlled mainly by the Pd deposition method, and thus, by Pd−ceria interaction promoting oxygen mobility, more than by the properties of ceria support, which, in turn, control the amount of stored NO_x. This result opens the way to the possibility of controlling the NO_x release process by properly tuning the Pd−Ce interaction, thus allowing the preparation of more efficient materials in which NO_x desorption mostly occurs within the operating window of the SCR catalyst.

4. CONCLUSIONS

In this study, 1 wt % Pd/CeO_2 materials were prepared by various synthesis techniques with different structural properties and were tested for passive NO_x adsorption at 373 K after lean and rich pretreatment in a dedicated microreactor setup.

The screening of these Pd/CeO_2 samples evidenced that the NO_x storage capacity is strictly related to their surface area: the higher the surface area, the higher the amount of stored NO_x both after 1 and after 30 min of adsorption. The geometry and the size of pores, instead, play a negligible role in the NO_x storage capacity. By comparing the results in terms of NO_x storage efficiency (NSE) during a short adsorption time, it has been possible to observe that after lean pretreatment, NSE improves as the surface area increases, with a slower decrease of NSE over time for high surface area samples. After a

https://doi.org/10.1021/acs.iecr.1c04805
Ind. Eng. Chem. Res. 2022, 61, 3329−3341

reducing pretreatment, instead, the samples supported on ceria nanorods display an NSE value close to those obtained for ceria nanoparticles having higher surface areas, indicating that on reduced samples likely a redox mechanism is also involved in NO_x adsorption, being more evident at the beginning of the adsorption step on materials with higher reducibility.

With respect to the desorption process, the dynamics of NO_x desorption is not governed by the distribution and shape of pores, nor by surface area, but mainly by the interaction between Pd and ceria. In particular, on Pd/CeO_2 materials, prepared by the solution combustion synthesis and dry milling, where Pd is in close contact with ceria increasing oxygen availability, most of stored NO_x desorb above 523 K while, on conventional impregnated samples, a larger amount of NO_x is released between 373 and 523 K. The strong Pd/ceria contact realized during the mechanical milling promotes the occurrence of a robust Pd−ceria interaction where Pd is embedded into CeO_2 surface layers.[37] Similarly, the formation of stable Pd−O−Ce surface structures characterizes SCS samples.[40] These highly active and stable sites, associated with higher oxygen mobility, might be more effective in oxidizing nitrites to more stable nitrates. This hypothesis seems corroborated by DRIFT measurements performed on two representative samples. The results evidenced that the milled sample is dominated by surface nitrate species, rather than nitrites, at a temperature lower than the impregnated counterpart and this can explain the different NO_x desorption efficiencies.

These findings highlight the key parameters necessary to control and optimize NO_x storage and desorption performance of Pd/CeO_2 materials, i.e., the high surface area to improve the NO_x storage capacity and a strong Pd−ceria interaction and oxygen mobility to obtain NO_x desorption in the appropriate temperature window, more favorable for the downstream de-NO_x processes.

■ ASSOCIATED CONTENT

Supporting Information

The Supporting Information is available free of charge at https://pubs.acs.org/doi/10.1021/acs.iecr.1c04805.

Details of synthesis procedures for the preparation of Pd/CeO_2 materials; a detailed list of prepared samples (Table S1); scheme of the reactor setup used for NO_x adsorption/desorption measurements (Figure S1); experimental protocol of NO_x adsorption/desorption tests (Figure S2); classification of the hysteresis loop during N_2 adsorption/desorption measurements (Figure S3); pore size distribution on some selected Pd/CeO_2 samples (Figure S4); XRD patterns of Pd/CeO_2 materials (Figures S5 and S6); CeO_2 crystal size of Pd/CeO_2 samples (Table S2); the HRTEM image of the high surface area dry milled Pd/CeO_2 sample (Figure S7); quantitative analysis of the NO_x adsorption/desorption test after lean and rich pretreatments (Tables S3 and S4); dependence of NO_x storage capacity on the textural properties of Pd/CeO_2 materials after rich pretreatment (Figure S8); H_2-TPR profile of some selected Pd/CeO_2 materials (Figure S9) and the corresponding quantitative analysis (Table S5); the NO_x desorption profile of Pd(iw)Ce(A)823F and Pd(m)Ce(A)823F after NO_x adsorption with 170 ppm NO and 30 ppm NO_2 at 373 K for 30 min (Figure S10); NO_x desorption profile for some selected impregnated, milled, and SCS Pd/CeO_2 samples after rich pretreatment (Figure S11); effect of the Pd deposition method on the amount of NO_x desorbed after rich pretreatment (Figure S12); NO_x desorption profile for Pd(iw)Ce(A)-823F and Pd(m)Ce(A)823F during isothermal desorption at 593 K for 1 h after lean pretreatment and the corresponding quantitative analysis (Figure S13 and Table S6); NO_x desorption profile for Pd(iw)Ce(A)-823F and Pd(m)Ce(A)823F after only NO and only NO_2 adsorption after lean pretreatment (Figure S14); quantitative analysis of NO_x desorbed with different NO_x adsorption feeds for Pd(iw)Ce(A)823F (Table S7) and Pd(m)Ce(A)823F (Table S8); NO_x released at $T <$ 523 K after adsorption in different NO_x feed (reactor setup) (Table S9); DRIFT spectra collected during NO + 8%O_2/N_2 and NO_2 + 8%O_2/N_2 adsorption at 373 K for 30 min on Pd(iw)Ce(A)823F and Pd(m)Ce(A)-823F (Figure S15); DRIFT spectra collected during TPD in 8% O_2/N_2 after NO + 8%O_2/N_2 or NO_2 + 8% O_2/N_2 adsorption (Figure S16); TPD in N_2 after NO + N_2 or NO_2 + N_2 adsorption (Figure S17) and after NO +NO_2/N_2 adsorption (Figure S18) (PDF)

■ AUTHOR INFORMATION

Corresponding Author

Sara Colussi − *Dipartimento Politecnico and INSTM, Università di Udine, 33100 Udine, Italy;* orcid.org/0000-0001-5316-1746; Email: sara.colussi@uniud.it

Authors

Alessandra Toso − *Dipartimento Politecnico and INSTM, Università di Udine, 33100 Udine, Italy;* orcid.org/0000-0002-4252-5978

Maila Danielis − *Dipartimento Politecnico and INSTM, Università di Udine, 33100 Udine, Italy;* orcid.org/0000-0001-8469-9282

Carla de Leitenburg − *Dipartimento Politecnico and INSTM, Università di Udine, 33100 Udine, Italy*

Marta Boaro − *Dipartimento Politecnico and INSTM, Università di Udine, 33100 Udine, Italy;* orcid.org/0000-0002-6853-2965

Alessandro Trovarelli − *Dipartimento Politecnico and INSTM, Università di Udine, 33100 Udine, Italy;* orcid.org/0000-0002-1396-4031

Complete contact information is available at: https://pubs.acs.org/10.1021/acs.iecr.1c04805

Notes

The authors declare no competing financial interest.

■ ACKNOWLEDGMENTS

This project was funded by Umicore AG & Co. KG under the Research Program "NO_x adsorbers based on Pd-ceria formulations: characterization and testing of new powder formulation for passive NO_x adsorption materials". The authors thank Prof. Jordi Llorca of the Institute of Energy Technologies, Department of Chemical Engineering, and Barcelona Research Centre in Multiscale Science and Engineering, Universitat Politécnica de Catalunya, for the HRTEM image.

REFERENCES

(1) Lambert, C. K. Current State of the Art and Future Needs for Automotive Exhaust Catalysis. *Nat. Catal.* **2019**, *2*, 554−557.

(2) Selleri, T.; Melas, A. D.; Joshi, A.; Manara, D.; Perujo, A.; Suarez-Bertoa, R. An Overview of Lean Exhaust DeNO$_x$ Aftertreatment Technologies and NO$_x$ Emission Regulations in the European Union. *Catalysts* **2021**, *11*, No. 404.

(3) Lai, J.-K.; Wachs, I. E. A Perspective on the Selective Catalytic Reduction (SCR) of NO with NH_3 by Supported V_2O_5−WO_3/TiO_2 Catalysts. *ACS Catal.* **2018**, *8*, 6537−6551.

(4) Han, L.; Cai, S.; Gao, M.; Hasegawa, J.; Wang, P.; Zhang, J.; Shi, L.; Zhang, D. Selective Catalytic Reduction of NO$_x$ with NH_3 by Using Novel Catalysts: State of the Art and Future Prospects. *Chem. Rev.* **2019**, *119*, 10916−10976.

(5) Andana, T.; Rappé, K. G.; Gao, F.; Szanyi, J.; Pereira-Hernandez, X.; Wang, Y. Recent Advances in Hybrid Metal Oxide−Zeolite Catalysts for Low-Temperature Selective Catalytic Reduction of NO$_x$ by Ammonia. *Appl. Catal., B* **2021**, *291*, No. 120054.

(6) Forzatti, P.; Lietti, L.; Castoldi, L. Storage and Reduction of NO$_x$ Over LNT Catalysts. *Catal. Lett.* **2015**, *145*, 483−504.

(7) Kim, B. S.; Jeong, H.; Bae, J.; Kim, P. S.; Kim, C. H.; Lee, H. Lean NO$_x$ Trap Catalysts with High Low-Temperature Activity and Hydrothermal Stability. *Appl. Catal., B* **2020**, *270*, No. 118871.

(8) Schmeisser, V.; Weibel, M.; Sebastian Hernando, L.; Nova, I.; Tronconi, E.; Ruggeri, M. P. Cold Start Effect Phenomena over Zeolite SCR Catalysts for Exhaust Gas Aftertreatment. *SAE Int. J. Commer. Veh.* **2013**, *6*, 190−199.

(9) Moliner, M.; Corma, A. From Metal-Supported Oxides to Well-Defined Metal Site Zeolites: The next Generation of Passive NO$_x$ Adsorbers for Low-Temperature Control of Emissions from Diesel Engines. *React. Chem. Eng.* **2019**, *4*, 223−234.

(10) Gu, Y.; Epling, W. S. Passive NO$_x$ Adsorber: An Overview of Catalyst Performance and Reaction Chemistry. *Appl. Catal., A* **2019**, *570*, 1−14.

(11) Jarvis, M.; Adams, K. M. Method for Converting Exhaust Gases from a Diesel Engine Using Nitrogen Oxide Absorbent. US6,182,443B1, 2001.

(12) Chen, H. Y.; Mulla, S.; Weigert, E.; Camm, K.; Ballinger, T.; Cox, J.; Blakeman, P. Cold Start Concept (CSC): A Novel Catalyst for Cold Start Emission Control. *SAE Int. J. Fuels Lubr.* **2013**, *6*, 372.

(13) Murata, Y.; Morita, T.; Wada, K.; Ohno, H. NO$_x$ Trap Three-Way Catalyst (N-TWC) Concept: TWC with NO$_x$ Adsorption Properties at Low Temperatures for Cold-Start Emission Control. *SAE Int. J. Fuels Lubr.* **2015**, *8*, 454−459.

(14) Ji, Y.; Bai, S.; Crocker, M. Al_2O_3-Based Passive NO$_x$ Adsorbers for Low Temperature Applications. *Appl. Catal., B* **2015**, *170*−*171*, 283−292.

(15) Chen, H.-Y.; Collier, J. E.; Liu, D.; Mantarosie, L.; Durán-Martín, D.; Novák, V.; Rajaram, R. R.; Thompsett, D. Low Temperature NO Storage of Zeolite Supported Pd for Low Temperature Diesel Engine Emission Control. *Catal. Lett.* **2016**, *146*, 1706−1711.

(16) Jones, S.; Ji, Y.; Crocker, M. Ceria-Based Catalysts for Low Temperature NO$_x$ Storage and Release. *Catal. Lett.* **2016**, *146*, 909−917.

(17) Ji, Y.; Bai, S.; Xu, D.; Qian, D.; Wu, Z.; Song, Y.; Pace, R.; Crocker, M.; Wilson, K.; Lee, A.; Harris, D.; Scapens, D. Pd-Promoted WO_3-ZrO_2 for Low Temperature NO$_x$ Storage. *Appl. Catal., B* **2020**, *264*, No. 118499.

(18) Kvasničková, A.; Kočí, P.; Ji, Y.; Crocker, M. Effective Model of NO$_x$ Adsorption and Desorption on PtPd/CeO_2-ZrO_2 Passive NO$_x$ Adsorber. *Catal. Lett.* **2020**, *150*, 3223−3233.

(19) Bian, C.; Li, D.; Liu, Q.; Zhang, S.; Pang, L.; Luo, Z.; Guo, Y.; Chen, Z.; Li, T. Recent Progress of Pd/Zeolite as Passive NO$_x$ Adsorber: Adsorption Chemistry, Structure-Performance Relationships, Challenges and Prospects. *Chin. Chem. Lett.* **2021**, DOI: 10.1016/J.CCLET.2021.07.066.

(20) Zhao, H.; Hill, A. J.; Ma, L.; Bhat, A.; Jing, G.; Schwank, J. W. Progress and Future Challenges in Passive NO Adsorption over Pd/Zeolite Catalysts. *Catal. Sci. Technol.* **2021**, *11*, 5986−6000.

(21) Lee, J.; Theis, J. R.; Kyriakidou, E. A. Vehicle Emissions Trapping Materials: Successes, Challenges, and the Path Forward. *Appl. Catal., B* **2019**, *243*, 397−414.

(22) Khivantsev, K.; Jaegers, N. R.; Kovarik, L.; Hu, J. Z.; Gao, F.; Wang, Y.; Szanyi, J. Palladium/Zeolite Low Temperature Passive NO$_x$ Adsorbers (PNA): Structure-Adsorption Property Relationships for Hydrothermally Aged PNA Materials. *Emiss. Control Sci. Technol.* **2020**, *6*, 126−138.

(23) Filtschew, A.; Stranz, D.; Hess, C. Mechanism of NO_2 Storage in Ceria Studied Using Combined in Situ Raman/FT-IR Spectroscopy. *Phys. Chem. Chem. Phys.* **2013**, *15*, 9066−9069.

(24) Filtschew, A.; Hess, C. Unravelling the Mechanism of NO and NO_2 Storage in Ceria: The Role of Defects and Ce-O Surface Sites. *Appl. Catal., B* **2018**, *237*, 1066−1081.

(25) Kim, Y.; Hwang, S.; Lee, J.; Ryou, Y.; Lee, H.; Kim, C. H.; Kim, D. H. Comparison of NO$_x$ Adsorption/Desorption Behaviors over Pd/CeO_2 and Pd/SSZ-13 as Passive NO$_x$ Adsorbers for Cold Start Application. *Emiss. Control Sci. Technol.* **2019**, *5*, 172−182.

(26) Trovarelli, A.; Fornasiero, P. *Catalysis by Ceria and Related Materials*, 2nd ed.; Catalytic Science Series; Imperial College Press: London, 2013; Vol. *12*.

(27) Montini, T.; Melchionna, M.; Monai, M.; Fornasiero, P. Fundamentals and Catalytic Applications of CeO_2-Based Materials. *Chem. Rev.* **2016**, *116*, 5987−6041.

(28) Khan, M. N.; Han, L.; Wang, P.; He, J.; Yang, B.; Yan, T.; Shi, L.; Zhang, D. SO_2-Tolerant NO$_x$ Reduction over Ceria-Based Catalysts: Shielding Effects of Hollandite Mn-Ti Oxides. *Chem. Eng. J.* **2020**, *397*, No. 125535.

(29) Guo, S.; Zhang, G.; Han, Z.-K.; Zhang, S.; Sarker, D.; Xu, W. W.; Pan, X.; Li, G.; Baiker, A. Synergistic Effects of Ternary PdO−CeO_2−OMS-2 Catalyst Afford High Catalytic Performance and Stability in the Reduction of NO with CO. *ACS Appl. Mater. Interfaces* **2021**, *13*, 622−630.

(30) Liu, B.; Liu, J.; Xin, L.; Zhang, T.; Xu, Y.; Jiang, F.; Liu, X. Unraveling Reactivity Descriptors and Structure Sensitivity in Low-Temperature NH_3-SCR Reaction over $CeTiO_x$ Catalysts: A Combined Computational and Experimental Study. *ACS Catal.* **2021**, *11*, 7613−7636.

(31) Theis, J. R.; Lambert, C. K. Mechanistic Assessment of Low Temperature NO$_x$ Adsorbers for Cold Start NO$_x$ Control on Diesel Engines. *Catal. Today* **2019**, *320*, 181−195.

(32) Hwang, S.; Kim, Y.; Lee, J.; Lee, E.; Lee, H.; Jeong, C.; Kim, C. H.; Kim, D. H. Promoting Effect of CO on Low-Temperature NO$_x$ Adsorption over Pd/CeO_2 Catalyst. *Catal. Today* **2022**, *384*−*386*, 88−96.

(33) Ilmasani, R. F.; Woo, J.; Creaser, D.; Olsson, L. Influencing the NO$_x$ Stability by Metal Oxide Addition to Pd/BEA for Passive NO$_x$ Adsorbers. *Ind. Eng. Chem. Res.* **2020**, *59*, 9830−9840.

(34) Gramigni, F.; Selleri, T.; Nova, I.; Tronconi, E. Catalyst Systems for Selective Catalytic Reduction + NO$_x$ Trapping: From Fundamental Understanding of the Standard SCR Reaction to Practical Applications for Lean Exhaust after-Treatment. *React. Chem. Eng.* **2019**, *4*, 1165−1178.

(35) Zheng, Y.; Kovarik, L.; Engelhard, M. H.; Wang, Y.; Wang, Y.; Gao, F.; Szanyi, J. Low-Temperature Pd/Zeolite Passive NO$_x$ Adsorbers: Structure, Performance, and Adsorption Chemistry. *J. Phys. Chem. C* **2017**, *121*, 15793−15803.

(36) Ohtake, N.; Katoh, M.; Sugiyama, S. High Thermal-Stability Ceria Synthesized via Thermal-Hydrolysis Route and Methane-Combustion Performance. *J. Ceram. Soc. Jpn.* **2017**, *125*, 57−61.

(37) Danielis, M.; Colussi, S.; de Leitenburg, C.; Soler, L.; Llorca, J.; Trovarelli, A. Outstanding Methane Oxidation Performance of Palladium-Embedded Ceria Catalysts Prepared by a One-Step Dry Ball-Milling Method. *Angew. Chem., Int. Ed.* **2018**, *57*, 10212−10216.

(38) Lowell, S.; Shields, J. E.; Thomas, M. A.; Thommes, M. *Characterization of Porous Solids and Powders: Surface Area, Pore Size*

https://doi.org/10.1021/acs.iecr.1c04805
Ind. Eng. Chem. Res. 2022, 61, 3329−3341

and Density; Particle Technology Series; Springer Netherlands: Dordrecht, 2004; Vol. *16*.
(39) Trovarelli, A.; Llorca, J. Ceria Catalysts at Nanoscale: How Do Crystal Shapes Shape Catalysis? *ACS Catal.* **2017**, *7*, 4716−4735.
(40) Colussi, S.; Gayen, A.; Camellone, M. F.; Boaro, M.; Llorca, J.; Fabris, S.; Trovarelli, A. Nanofaceted Pd-O Sites in Pd-Ce Surface Superstructures: Enhanced Activity in Catalytic Combustion of Methane. *Angew. Chem., Int. Ed.* **2009**, *48*, 8481−8484.
(41) Azambre, B.; Zenboury, L.; Koch, A.; Weber, J. V. Adsorption and Desorption of NO_x on Commercial Ceria-Zirconia ($Ce_xZr_{1-x}O_2$) Mixed Oxides: A Combined TGA, TPD-MS, and DRIFTS Study. *J. Phys. Chem. C* **2009**, *113*, 13287−13299.
(42) Zou, X.; Rui, Z.; Ji, H. Core-Shell NiO@PdO Nanoparticles Supported on Alumina as an Advanced Catalyst for Methane Oxidation. *ACS Catal.* **2017**, *7*, 1615−1625.
(43) Ryou, Y. S.; Lee, J.; Lee, H.; Kim, C. H.; Kim, D. H. Low Temperature NO Adsorption over Hydrothermally Aged Pd/CeO_2 for Cold Start Application. *Catal. Today* **2018**, *307*, 93−101.
(44) Danielis, M.; Betancourt, L. E.; Orozco, I.; Divins, N. J.; Llorca, J.; Rodríguez, J. A.; Senanayake, S. D.; Colussi, S.; Trovarelli, A. Methane Oxidation Activity and Nanoscale Characterization of Pd/CeO_2 Catalysts Prepared by Dry Milling Pd Acetate and Ceria. *Appl. Catal., B* **2021**, *282*, No. 119567.
(45) Theis, J. R. An Assessment of Pt and Pd Model Catalysts for Low Temperature NO_x Adsorption. *Catal. Today* **2016**, *267*, 93−109.
(46) Hadjiivanov, K. I. Identification of Neutral and Charged N_xO_y Surface Species by IR Spectroscopy. *Catal. Rev.: Sci. Eng.* **2000**, *42*, 71−144.
(47) Zhang, L.; Pierce, J.; Leung, V. L.; Wang, D.; Epling, W. S. Characterization of Ceria's Interaction with NO_x and NH_3. *J. Phys. Chem. C* **2013**, *117*, 8282−8289.
(48) Mihaylov, M. Y.; Ivanova, E. Z.; Vayssilov, G. N.; Hadjiivanov, K. I. Revisiting Ceria-NO_x Interaction: FTIR Studies. *Catal. Today* **2020**, *357*, 613−620.
(49) Martínez-Arias, A.; Soria, J.; Conesa, J. C.; Seoane, X. L.; Arcoya, A.; Cataluña, R. NO Reaction at Surface Oxygen Vacancies Generated in Cerium Oxide. *J. Chem. Soc., Faraday Trans.* **1995**, *91*, 1679−1687.

https://doi.org/10.1021/acs.iecr.1c04805
Ind. Eng. Chem. Res. 2022, 61, 3329−3341